Supplement of Atmos. Chem. Phys., 24, 5099–5115, 2024
https://doi.org/10.5194/acp-24-5099-2024-supplement

Atmospheric Chemistry and Physics
Open Access
EGU

Supplement of

Role of the Indian Ocean basin mode in driving the interdecadal variations of summer precipitation over the East Asian monsoon boundary zone

Jing Wang et al.

Correspondence to: Yanju Liu (liuyanj@cma.gov.cn)

Glossary of acronyms

20CRv2c	Twentieth Century Reanalysis version 2c
CESM1	Community Earth System Model version 1
CESM1_IOPES	CESM1 Indian Ocean Pacemaker Ensemble Simulation
CESM1_LENS	CESM1 Large Ensemble Numerical Simulation
CIRES	Cooperative Institute for Research in Environmental Sciences
CRU	Climatic Research Unit
EAMBZ	East Asian monsoon boundary zone
EASM	East Asian summer monsoon
EOF	Empirical orthogonal function
ERSSTv5	Extended Reconstructed sea surface temperature version 5
IOBM	Indian Ocean basin mode
IPO	Interdecadal Pacific oscillation
JJA	June–July–August
NCAR	National Center for Atmospheric Research
NOAA	National Oceanic and Atmospheric Administration
RWS	Rossby wave source
SST	Sea surface temperature
SSTAs	SST anomalies
SWP	Subtropical western Pacific
SWPCGA	SWP clockwise gyre anomaly
TCC	Temporal correlation coefficient
TIO	Tropical Indian Ocean
TP	Tibetan Plateau
WVT	Water vapor transport
WVT_div	WVT-associated divergence

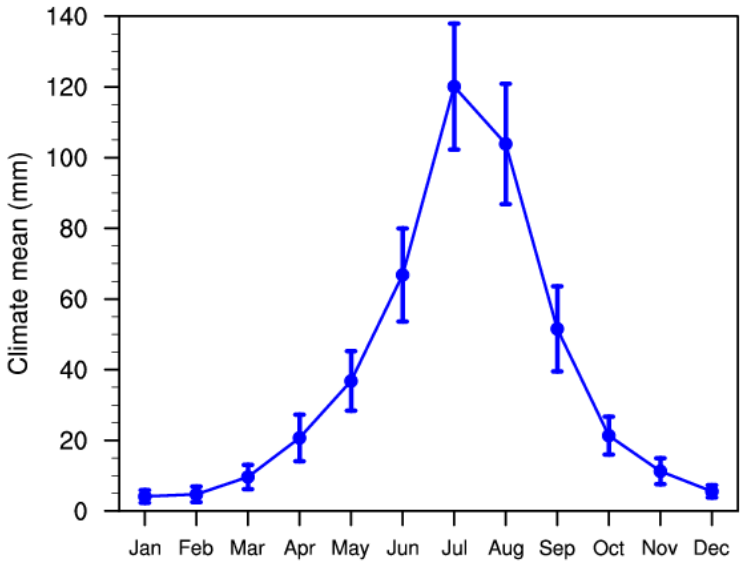

Figure S1. Annual cycle of the climatological-mean (1901–2014) EAMBZ precipitation (mm). The error bars denote one standard deviation from the mean. The precipitation is derived from the CRU TS3.26 precipitation data.

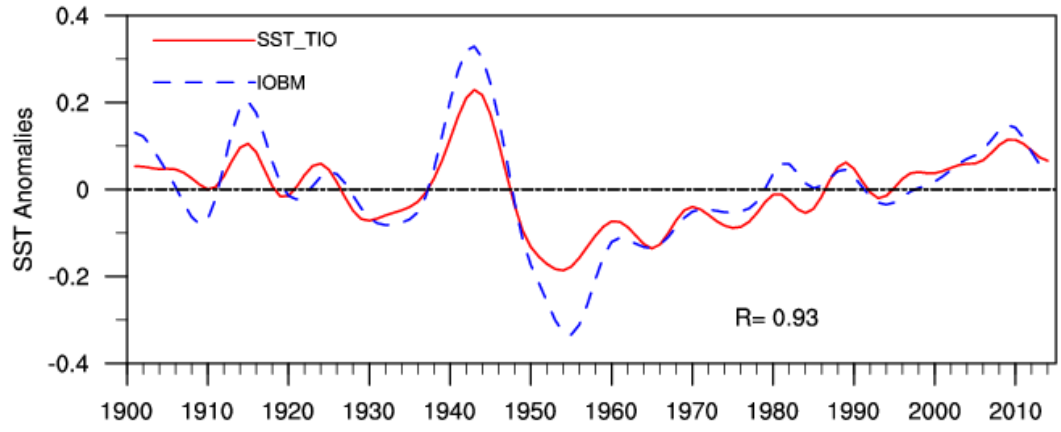

Figure S2. Time-evolving observed summertime SSTAs over the narrower TIO domain for defining I_{IOBM} (20 °S–20 °N, 40 °–100 °E; blue line) and SSTAs over the broader TIO domain in CESM1_IOPES (15 °S–15 °N, 40 °–174 °E; red line) from 1901–2014. The time series are detrended and 11-year low-pass filtered. The numeral at the bottom represents the TCC between the corresponding time series. The base period for calculating SSTAs is 1901–2014. The areal mean SSTAs are calculated based on the ERSSTv5.

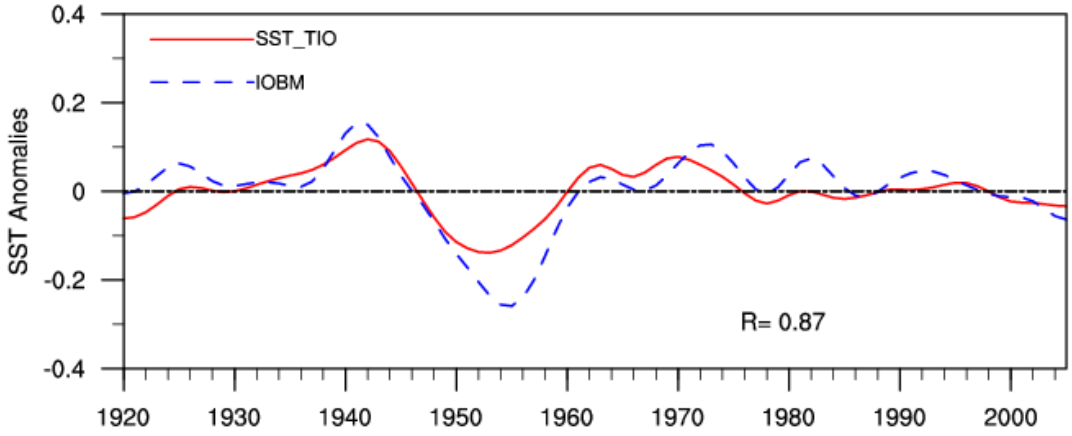

Figure S3. Time-evolving simulated summertime SSTAs over the narrower TIO domain for defining I_{IOBM} (20 °S–20 °N, 40 °–100 °E; blue line) and SSTAs over the broader TIO domain in CESM1_IOPES (15 °S–15 °N, 40 °–174 °E; red line) from 1920–2005. The time series are detrended and 11-year low-pass filtered. The numeral at the bottom represents the TCC between the corresponding time series. The areal mean SSTAs are calculated based on the difference between the CESM1_IOPES ensemble mean and the CESM1_LENS ensemble mean (former minus latter).

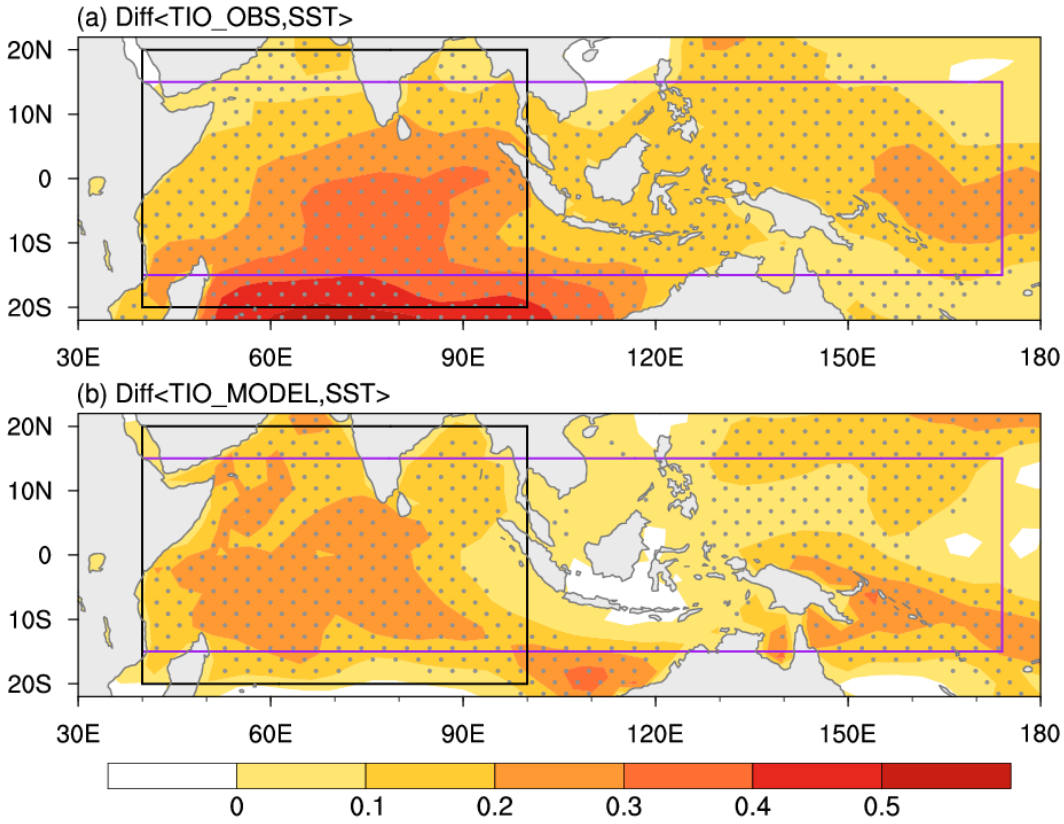

Figure S4. Composite differences of (a) observed and (b) simulated JJA-mean SST (℃) between warm and cold SST years over the broader TIO domain in CESM1_IOPES (15 ℃S–15 ℃N, 40 °–174 ℃E; purple box). In panel (a), the warm and cold TIO SST years are selected based on the ±0.5 standard deviations of the observed time-evolving SSTAs during 1901–2014, as shown in Fig. S2 (red line). In panel (b), the warm and cold TIO SST years are selected based on the ±0.5 standard deviations of the simulated time-evolving SSTAs during 1920–2005, as shown in Fig. S3 (red line). The black frame (20 ℃S–20 ℃N, 40 °–100 ℃E) outlines the domain for delineating the IOBM mode (the same hereinafter). All variables are detrended and 11-year low-pass filtered. Areas with significant values exceeding the 95% confidence level are dotted. The observed SSTAs are derived from the ERSSTv5; whilst the simulated SSTAs are calculated based on the difference between the CESM1_IOPES ensemble mean and the CESM1_LENS ensemble mean (former minus latter), highlighting the internally driven impacts of TIO SSTAs.

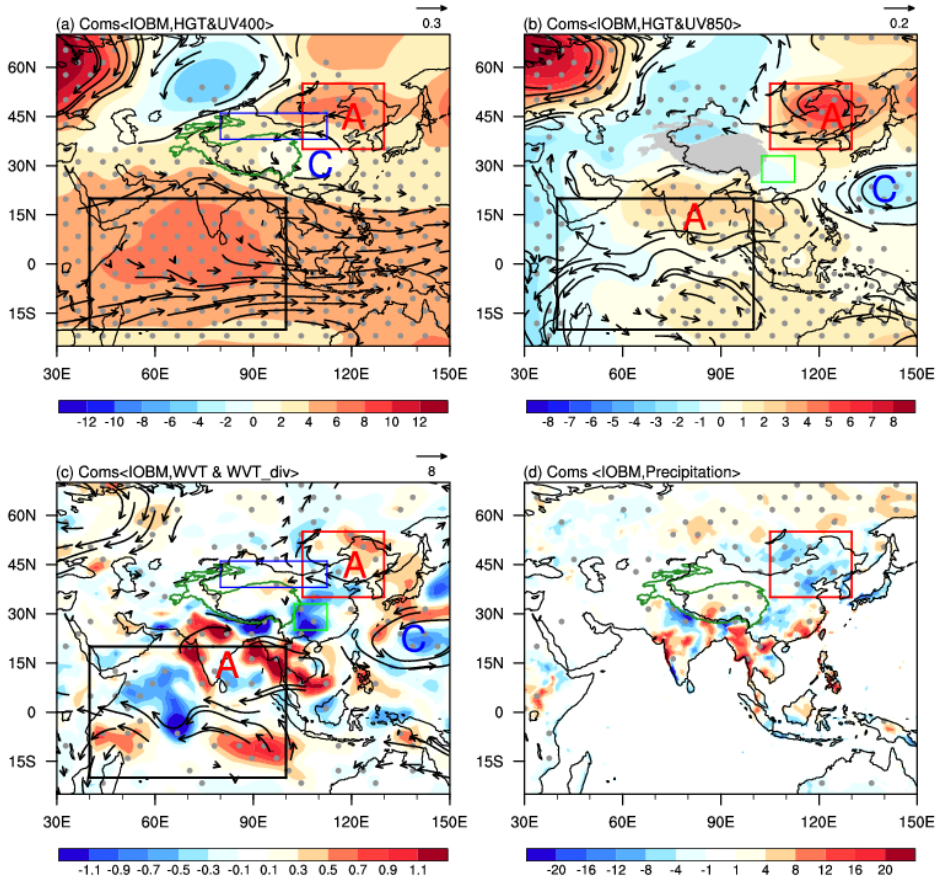

Figure S5. Composite anomalies of JJA-mean (a) Z400 (shading; m) and UV400 (vectors; m s^{-1}), (b) Z850 (shading; m) and UV850 (vectors; m s^{-1}), (c) <WVT> (vectors; kg m^{-1} s^{-1}) and <WVT_div> (shading; 10^{-5} kg m^{-2} s^{-1}), and (d) precipitation (mm $month^{-1}$) during the warm phase years of the IOBM. All variables are detrended and 11-year low-pass filtered. Areas with significant values of Z400, Z850, and <WVT_div> that exceed the 95% confidence level are stippled, respectively. Only vectors that are significant at the 95% confidence level are shown. The base period is 1901–2014. The warm phase years of the IOBM are selected based on the 0.5 standard deviations of the observed time-evolving SSTAs during the based period, as shown in Fig. 6b (blue line). The precipitation is derived from the CRU TS3.26 precipitation data; whilst other variables are from the 20CRv2c datasets.

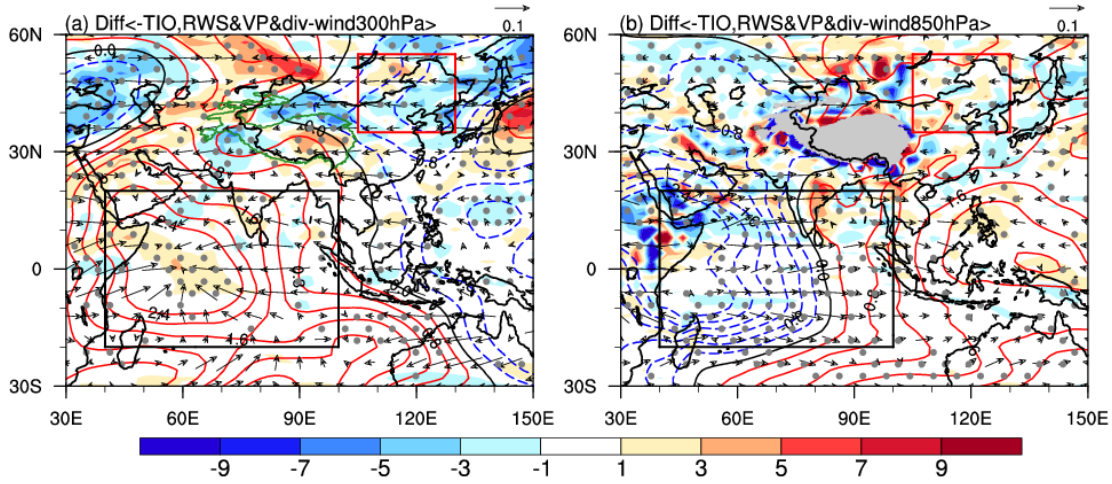

Figure S6. Simulated composite differences of JJA-mean (a) 300- and (b) 850-hPa RWS (shading; 10^{-11} s^{-2}), velocity potential (contours; interval: 0.8; 10^5 m^2 s^{-1}), and divergent horizontal wind (vectors; m s^{-1}) between cold and warm SST years over the broader TIO domain in CESM1_IOPES (15 °S–15 °N, 40 °–174 °E; purple box in Fig. S4). The warm and cold TIO SST years are selected based on the ±0.5 standard deviations of the simulated time-evolving SSTAs during 1920–2005, as shown in Fig. S3 (red line). All variables are detrended and 11-year low-pass filtered. Areas with significant values of RWS exceeding the 95% confidence level are stippled. Only vectors that are significant at the 95% confidence level are shown. The simulated anomalies of RWS, velocity potential, and divergent horizontal wind are calculated based on the difference between the CESM1_IOPES ensemble mean and the CESM1_LENS ensemble mean (former minus latter), highlighting the internally driven impacts of TIO SSTAs.